Supporting Information

Construction of covalent organic frameworks from nanosphere for Cu^{2+}detection

Wenyue Ma, Zijian Gu, Canran Wang, Liangyu Dong, Zhaoyang Liu, Leijing Liu,

Bin Xu and Wenjing Tian*

State Key Laboratory of Supramolecular Structure and Materials, College of Chemistry, Jilin University,

Changchun 130012, China

Correspondence: wjtian@jlu.edu.cn

1. Instrumentations

The solid-state ^{13}C cross-polarization/magic-angle spinning (CP/ MAS) NMR spectra were collected using a Bruker AVANCE III 400 WB spectrometer. The time-of-flight mass spectra were recorded using a Kratos MALDI-TOF mass system. Fourier transform infrared (FT-IR) spectra were recorded on a Vertex 80 V spectrometer. The samples were grinded into powder and dried, then mixed with dried KBr (powder) and pressed into piece. UV-Vis spectra were recorded with a Shimadzu UV-2550 spectrophotometer. Fluorescence spectroscopy was taken using a Shimadzu RF-5301 PC spectrometer. SEM images were recorded using scanning electron microscopy (Hitachi Regulus 8100). A drop of the aqueous solution was dripped directly onto a silicon wafer and air-dried. The TEM images were recorded using a JEM-2100F instrument with an accelerating voltage of 200 kV. The samples were prepared by placing a drop of the stock solution on a 300-mesh, carbon-coated copper grid and air-dried before measurement. The N_2 adsorption–desorption isotherms were measured using a Quantachrome Autosorb-iQ2 analyzer. Powder X-ray diffraction (PXRD) was performed with a Riguku D/MAX2550 diffractometer using Cu-Kα radiation, 40 kV, 200 mA at room temperature.

2. Synthesis of TFPB-ED HS

The synthetic method of TFPB-ED HS was performed according to previous literature [1].

3. Synthesis of TFPB-DETH COF

TFPB (19.522 mg) and DETH (21.17 mg) were mixed in the presence of mesitylene / dioxane / 6 M AcOH (6/4/1 by vol.; 1.1 mL) in a Pyrex tube (10 mL), which was degassed by three freeze-

pump-thaw cycles. The tube was sealed off and heated at 120 ℃ for 3 days. The production was collected by centrifugating and washing with anhydrous THF several times. The resulting powder was pale yellow powder.

4. Synthesis of Transformed-TFPB-DETH COF

TFPB-ED HS (5 mg) and DETH (6.4 mg) were mixed in the presence of mesitylene / dioxane / 6 M AcOH (6/4/1 by vol.; 1.1 mL) in a Pyrex tube (10 mL), which was degassed by three freeze-pump-thaw cycles. The tube was sealed off and heated at 120 ℃ for 3 days. The production was collected by centrifugating and washing with anhydrous THF and acetone several times. The resulting powder was pale yellow powder. Transformed-TFPB-BTA COF and Transformed-TFPB-DHz COF were prepared by the mixed solution of mesitylene and dioxane.

5. Quantum yield determination of the Transformed-TFPB-DETH COF

First, we select the integrating sphere attachment and the solvent test mode. Then, the fluorescence spectra of the blank solvent and the COF suspension (0.33 mg / mL) are measured with the excitation wavelength of 365 nm. Finally, data fitting is performed to obtain quantum efficiency data.

6. Molecular simulation

The lattice model was optimized through using the Materials Studio Forcite molecular dynamics module under ultra-fine, Universal force fields, Ewald summations condition to determine the structure of Transformed-TFPB-DETH COF, Transformed-TFPB-BTA COF and Transformed-TFPB-DHz COF. Then Pawley refinements were conducted using Reflex to fit profiles of PXRD.

7. Sensing Experiment of the Transformed- COFs toward Cu^{2+}

Stock solution of the Transformed-COFs (1 mg/mL) were prepared by dispersing fine powder of the Transformed-COFs in EtOH. The mixed solutions were sonicated for a while to produce homogeneous suspensions and used for luminescent measurements. The sensing experiments were performed by adding aqueous solutions of chloride metal salts at specific concentrations into 3 mL the COF suspension at room temperature and recording the luminescence data immediately.

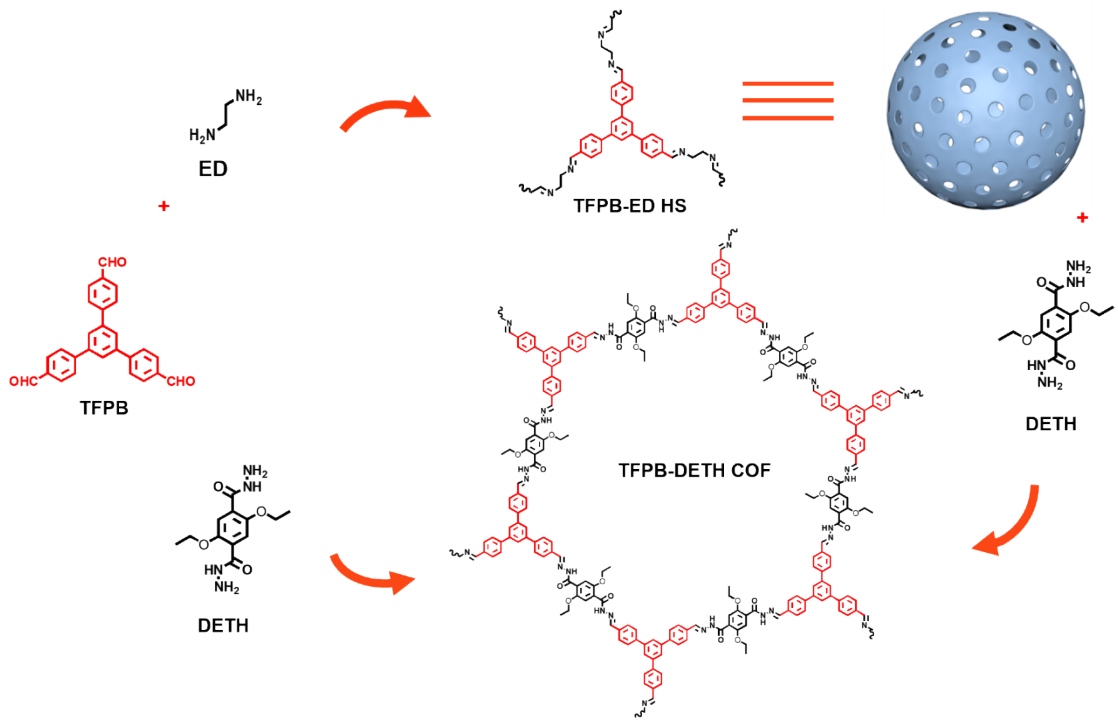

Fig. S1. Synthesis routes of TFPB-ED HS and the COF.

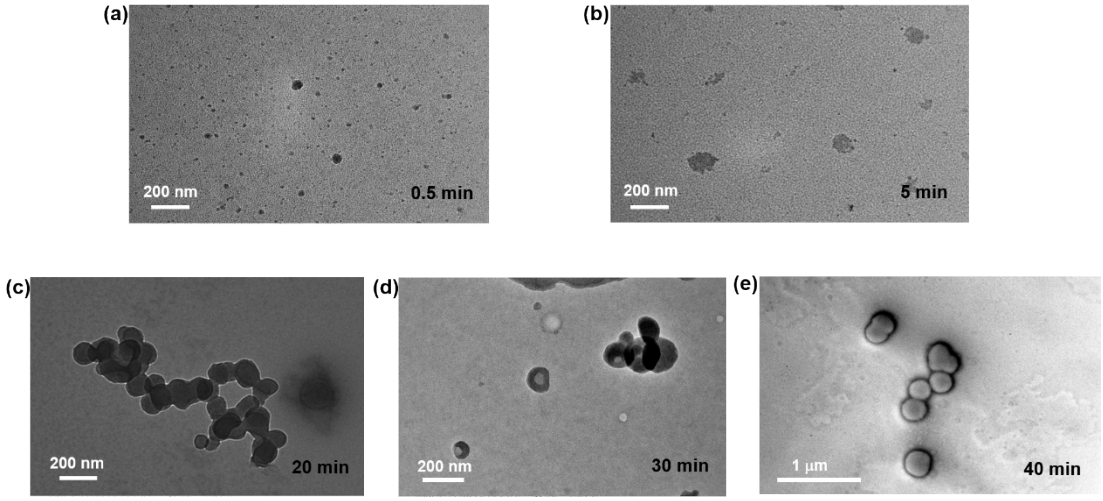

Fig. S2. TEM images of the growth of nanospheres at different times.

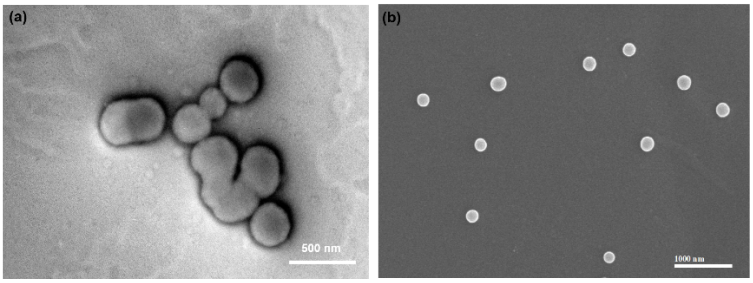

Fig. S3. (a) TEM image of the nanosphere, (b) SEM image of the nanosphere.

Table S1. Synthesis of the Transformed-TFPB-DETH COF under different solvothermal conditions.

Solvent (1 mL)	Catalyst (0.1 mL)	Temperature
Dioxane:mesitylene=3:2	6.0 mol/L HAc	120 ℃
Dioxane:mesitylene=1:2		
Dioxane:mesitylene=1:3		
Dioxane:mesitylene=1:1		
Dioxane		
Mesitylene		
Dioxane:mesitylene=3:2	6.0 mol/L HAc	90 ℃
Dioxane:mesitylene=1:2		
Dioxane:mesitylene=1:3		
Dioxane:mesitylene=1:1		

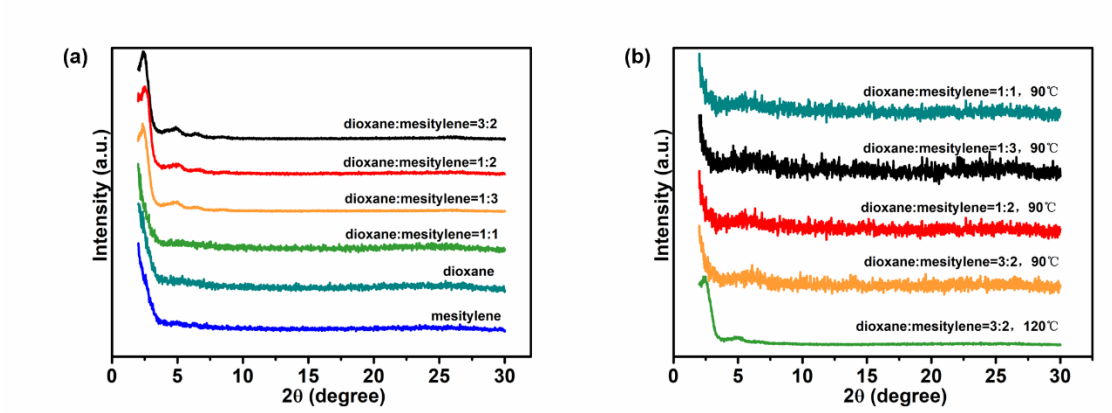

Fig. S4. (a) XRD patterns of the Transformed-TFPB-DETH COF in various reacting solvents, (b) XRD patterns of the Transformed-TFPB-DETH COF in different reacting temperatures.

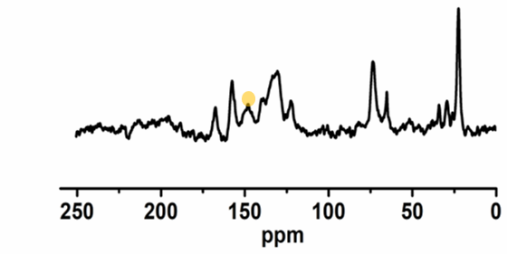

Fig. S5. Solid-state ^{13}C NMR spectrum of the Transformed-TFPB-DETH COF.

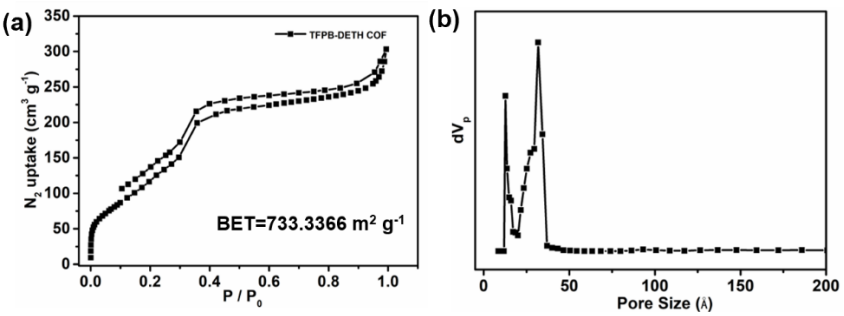

Fig. S6. (a) N_2 adsorption/ desorption isotherms, (b) pore size distribution of the Transformed-TFPB-DETH COF.

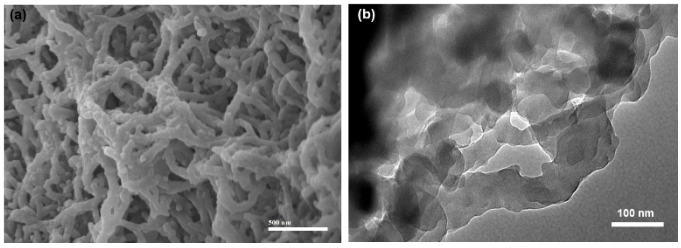

Fig. S7. (a) SEM image of the Transformed-TFPB-DETH COF, (b) TEM image of the Transformed-TFPB-DETH COF.

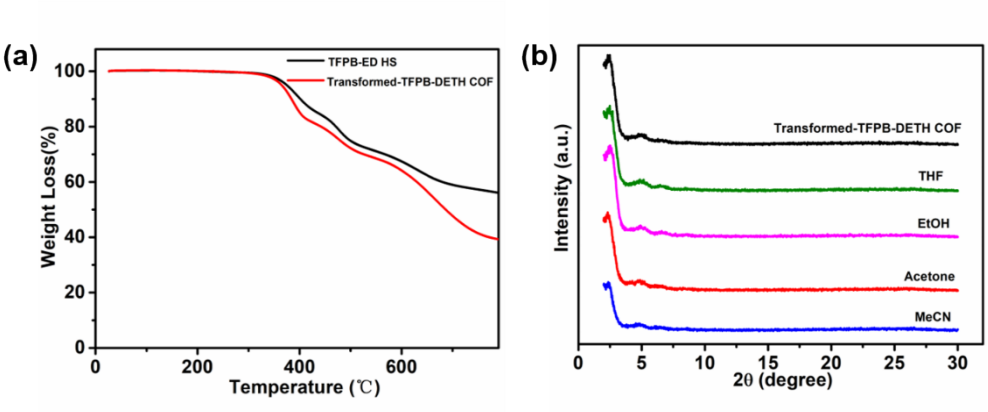

Fig. S8. (a) TGA curves of the Transformed-TFPB-DETH COF and TFPB-ED HS, (b) XRD patterns of the Transformed-TFPB-DETH COF after immersion in various solvents for 72 h.

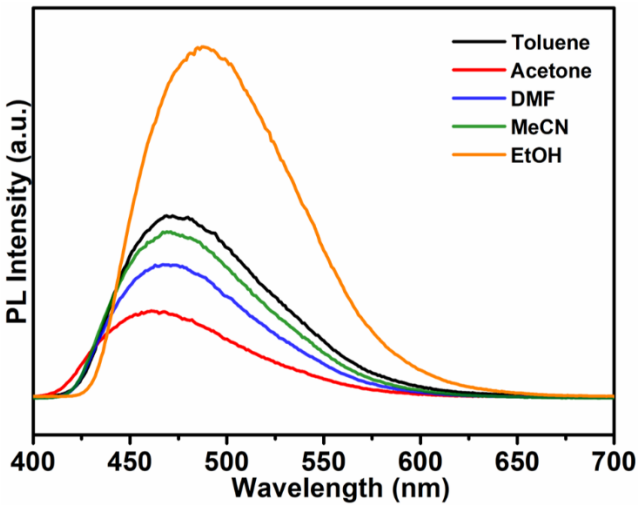

Fig. S9. PL spectrum of the Transformed-TFPB-DETH COF in different solvents.

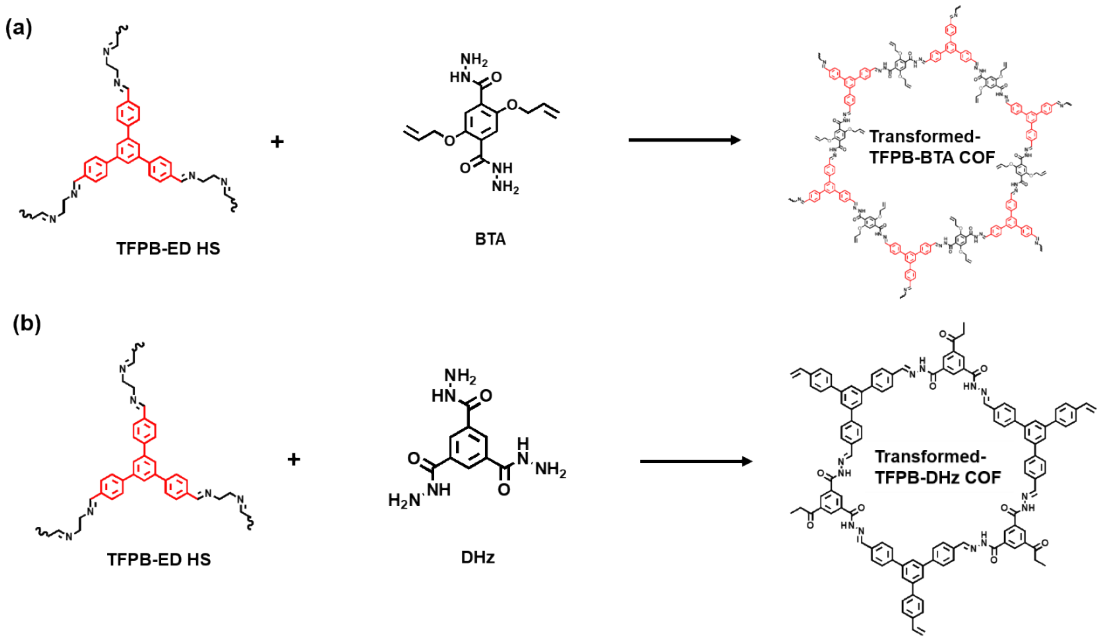

Fig. S10. Synthesis routes of (a) the Transformed-TFPB-BTA COF, (b) the Transformed-TFPB-DHz COF.

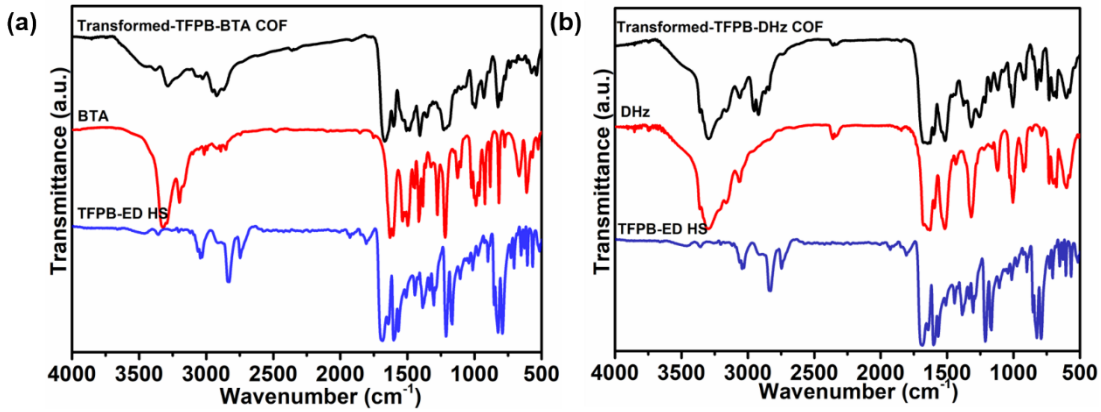

Fig. S11. FT IR spectra of (a) the Transformed-TFPB-BTA COF, (b) the Transformed-TFPB-DHz COF.

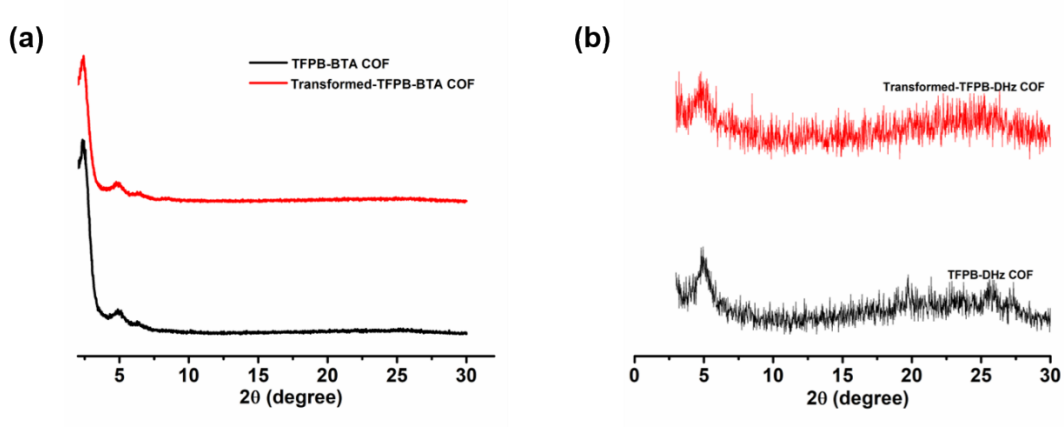

Fig. S12. PXRD profiles of (a) the Transformed-TFPB-BTA COF, (b) the Transformed-TFPB-DHz COF.

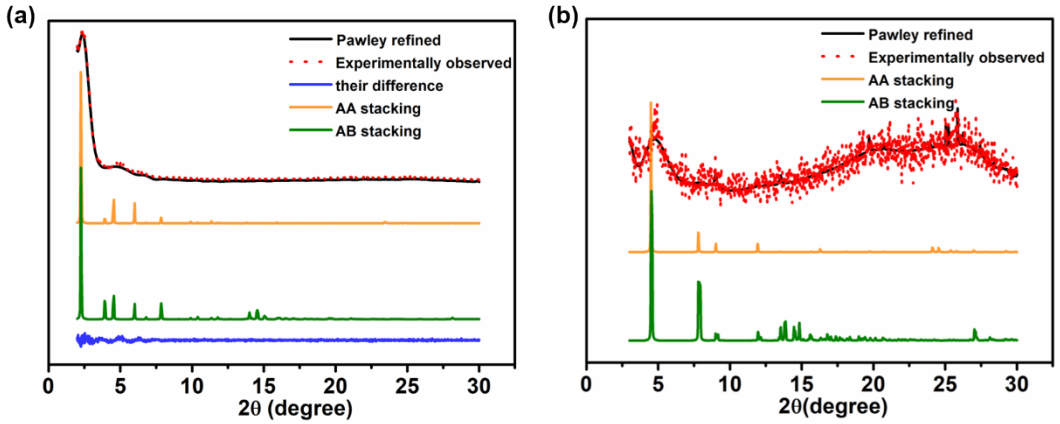

Fig. S13. (a) PXRD profiles of the Transformed-TFPB- BTA COF of the experimentally observed (red), Pawley refined (black) and their difference (blue), simulated using the AA (orange) stacking

mode, simulated using the AB (green) stacking mode, (b) PXRD profiles of the Transformed-TFPB-DHz COF of the experimentally observed (red), Pawley refined (black), simulated using the AA (orange) stacking mode, simulated using the AB (green) stacking mode.

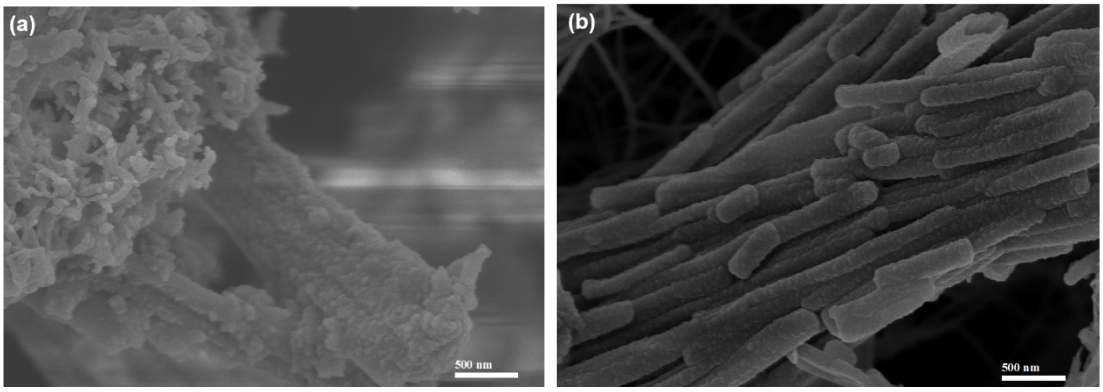

Fig. S14. SEM images of (a) the Transformed-TFPB-BTA COF, (b) the Transformed-TFPB-DHz COF.

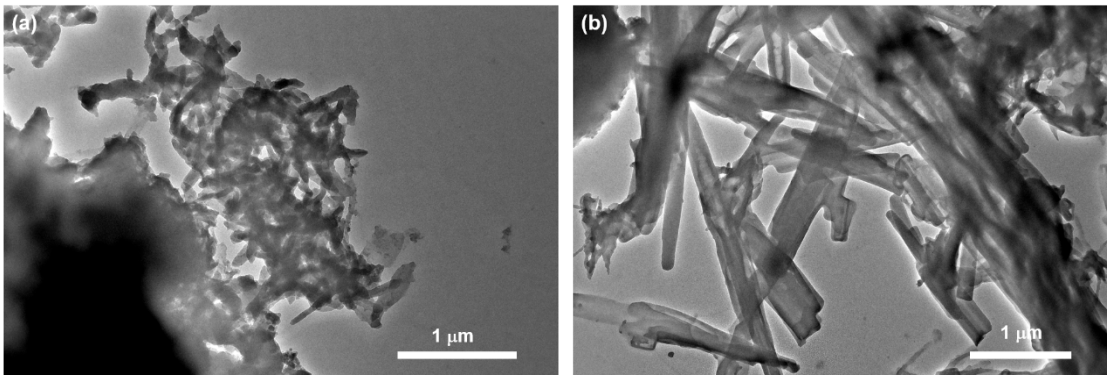

Fig. S15. TEM images of (a) the Transformed-TFPB-BTA COF, (b) the Transformed-TFPB-DHz COF.

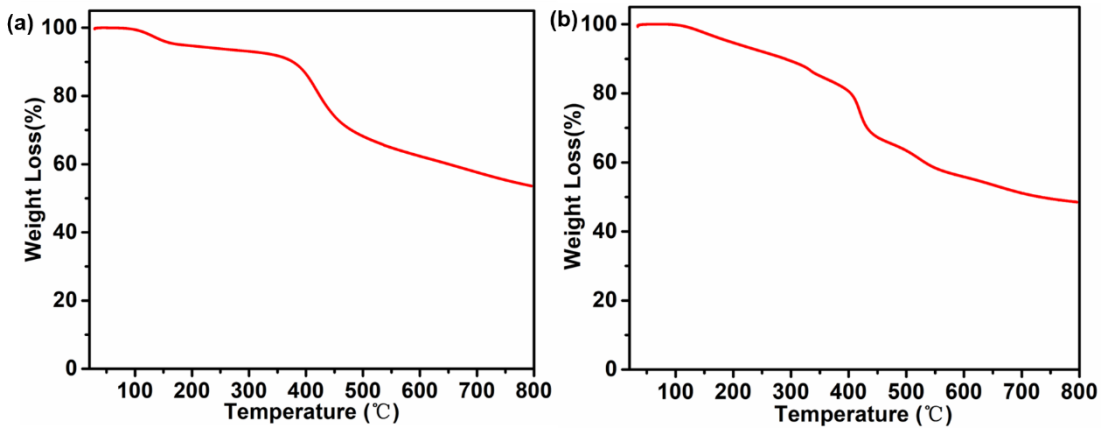

Fig. S16. TGA curve of (a) the Transformed-TFPB-BTA COF, (b) the Transformed-TFPB-DHz COF.

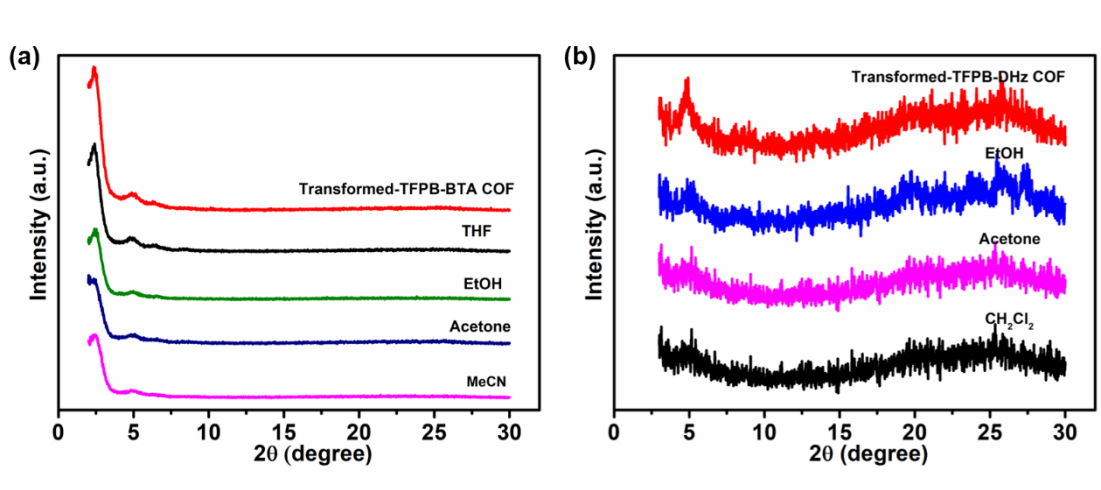

Fig. S17. XRD patterns of (a) the Transformed-TFPB-BTA COF, (b) the Transformed-TFPB-DHz COF after immersing in various solvents for 72 h.

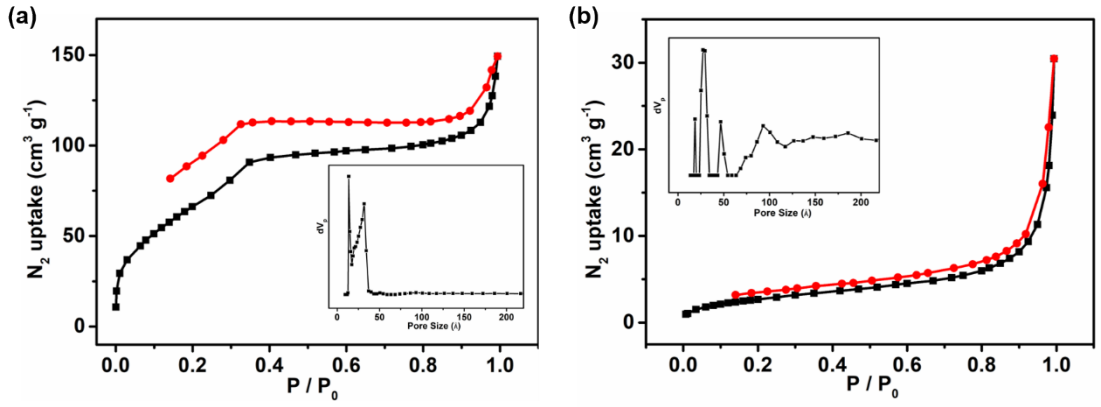

Fig. S18. N_2 adsorption / desorption isotherms of (a) the Transformed-TFPB-BTA COF, (b) the Transformed-TFPB-DHz COF (inset: pore size distribution). BET surface of the Transformed-

TFPB-DHz COF is poor, which is attributed to the low crystallinity.

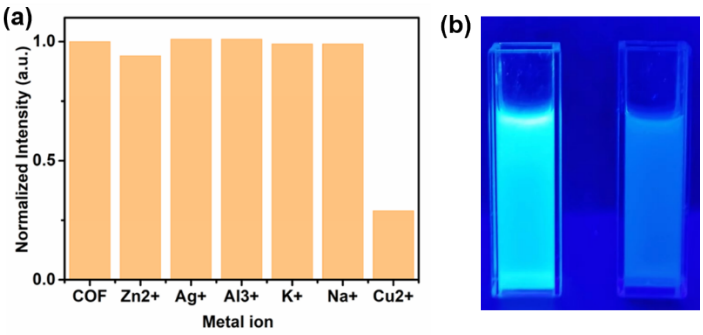

Fig. S19. (a) Comparison of the luminescence intensity of the Transformed-TFPB-DETH COF in the presence of various metal ions (24.8μmol / L) in EtOH (λ_{ex} = 365 nm), (b) a photo showing fluorescence change (under a UV lamp with λ_{ex} = 365 nm) of the Transformed-COF in EtOH upon addition of 24.8 μmol / L of Cu^{2+}.

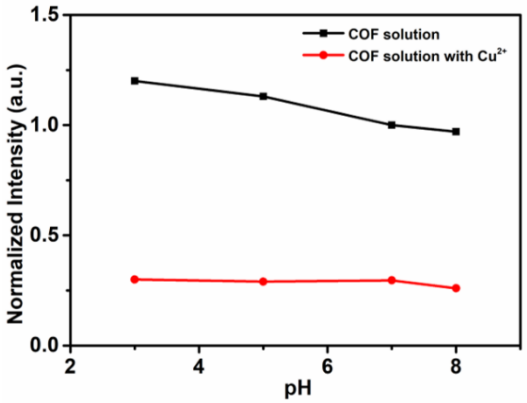

Fig. S20. Effect of pH on the detection of Cu^{2+} for the Transformed-TFPB-DETH COF.

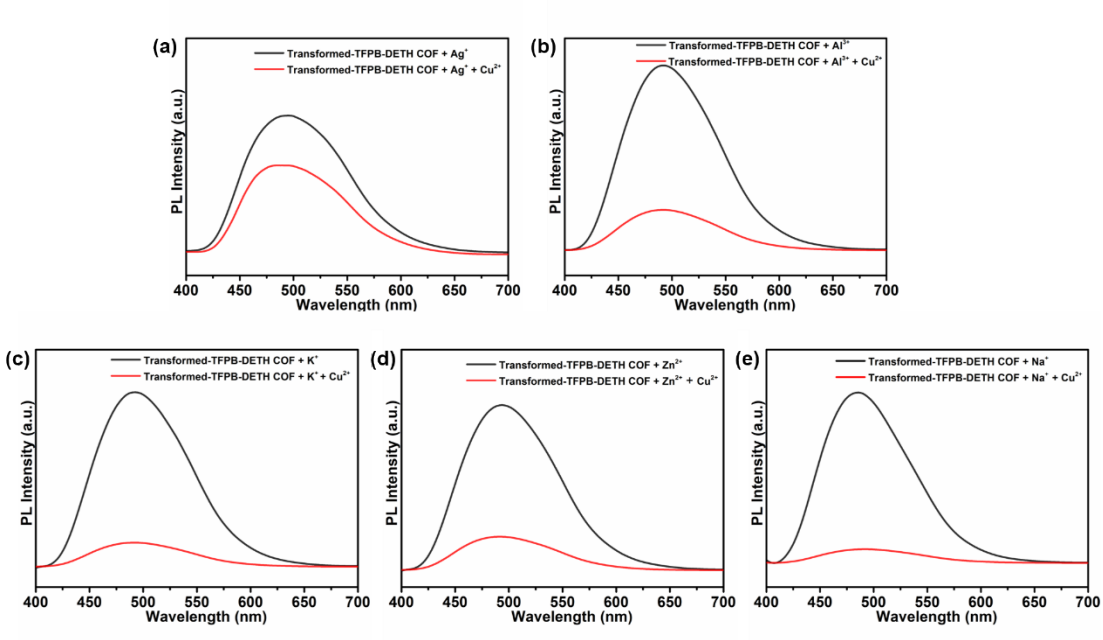

Fig. S21. Effect of different metal ions on the detection of Cu^{2+} for the Transformed-TFPB-DETH COF.

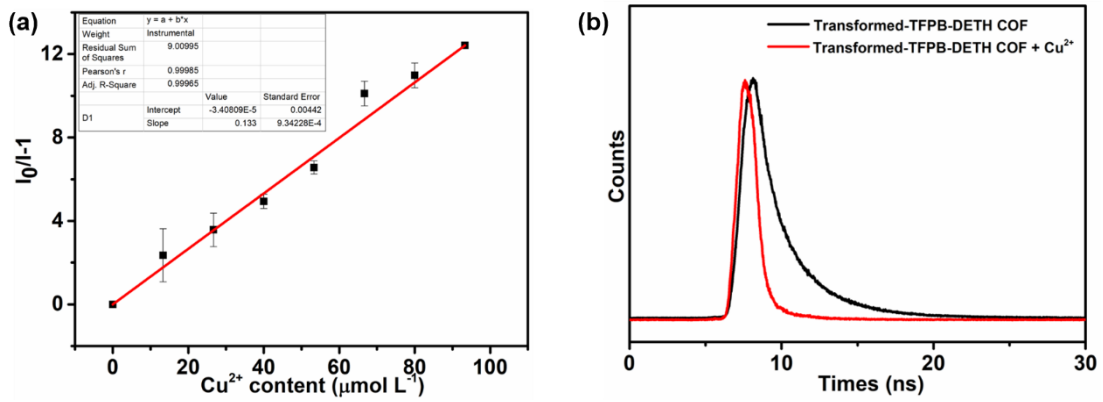

Fig. S22. (a) The linear correlation between the fluorescence change of Transformed-TFPB-DETH COF and different concentrations of Cu^{2+} in EtOH (R^2=0.999), (b) fluorescence lifetime of the Transformed-TFPB-DETH COF before and after adding Cu^{2+}.

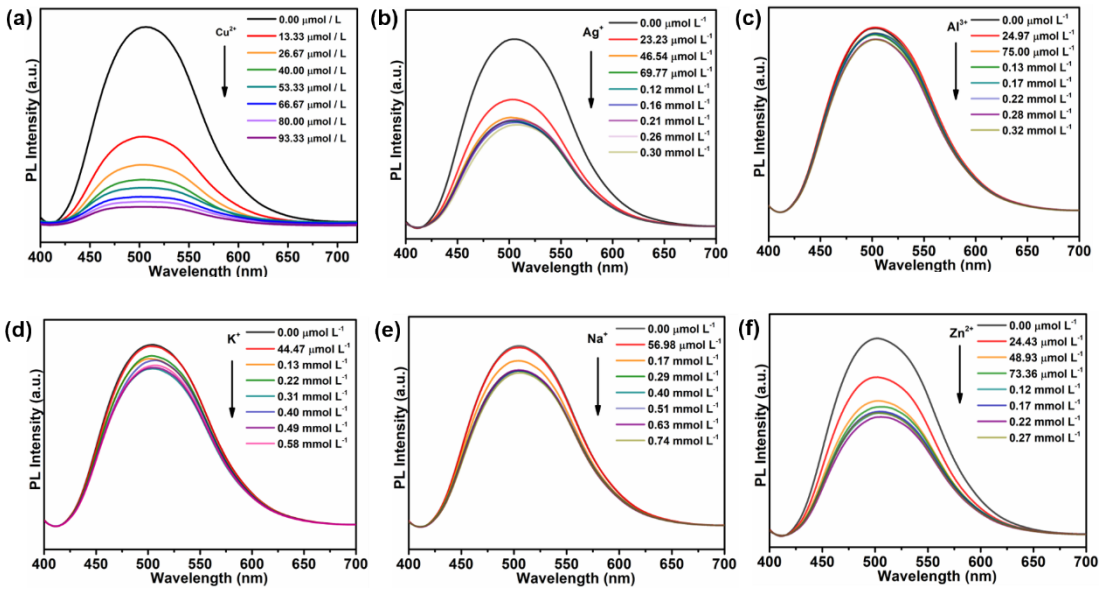

Fig. S23. Emission spectra of the Transformed-TFPB-BTA COF in EtOH suspensions containing various contents of (a) Cu^{2+}, (b) Ag^{+}, (c) Al^{3+}, (d) K^{+}, (e) Na^{+}, (f) Zn^{+}.

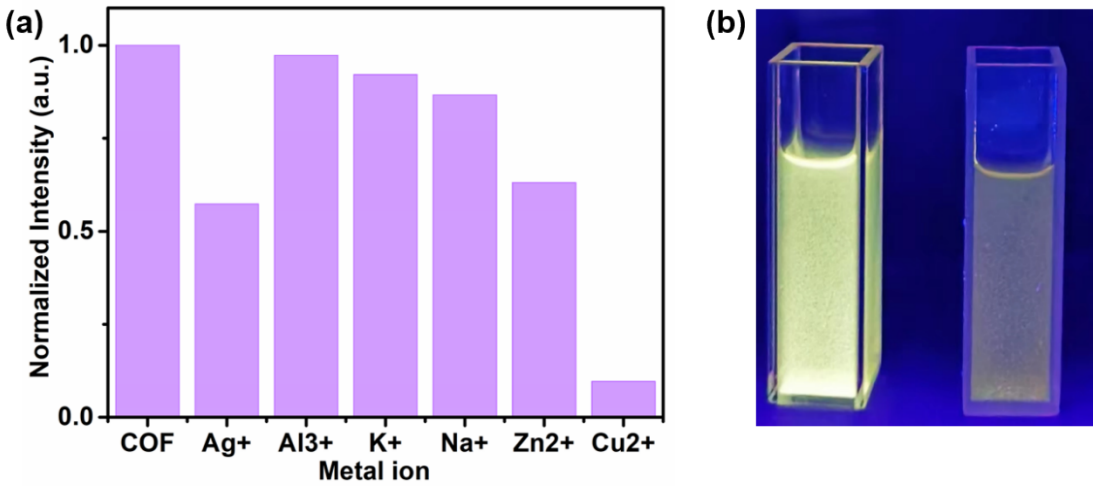

Fig. S24. (a) Comparison of the luminescence intensity of the Transformed-TFPB-BTA COF in the presence of various metal ions (0.12 mmol / L) in EtOH (λ_{ex} = 365 nm), (b) A photo showing fluorescence change (under a UV lamp with λ_{ex} = 365 nm) of the Transformed-TFPB-BTA COF in EtOH upon addition of 0.12 mmol / L of Cu^{2+}.

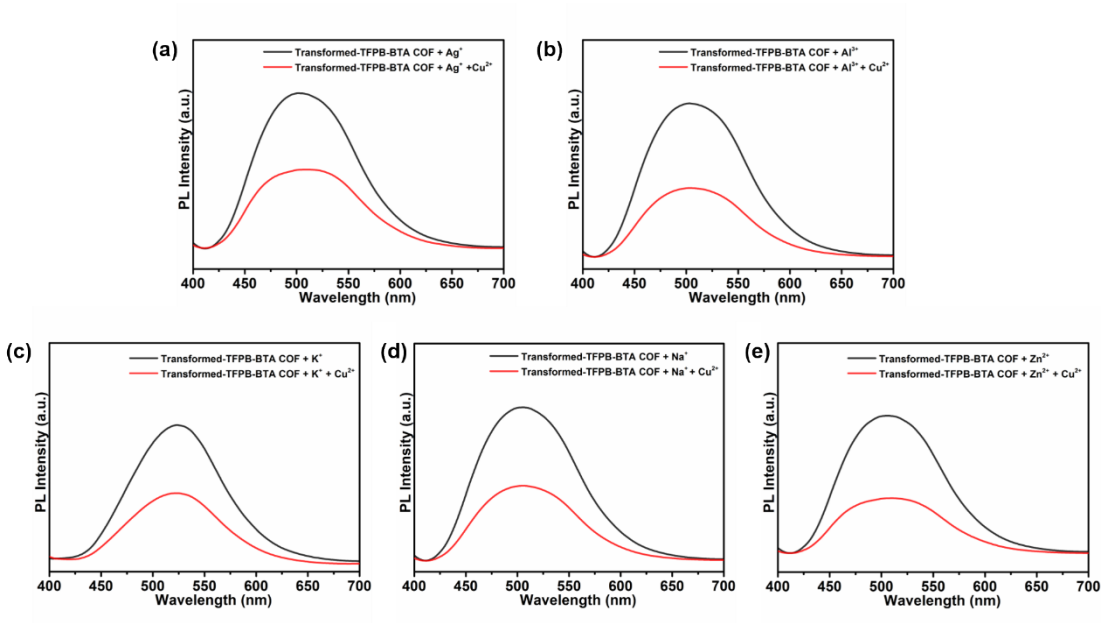

Fig. S25. Effect of different metal ions (100 mmol) on the detection of Cu^{2+} for the Transformed-TFPB-BTA COF.

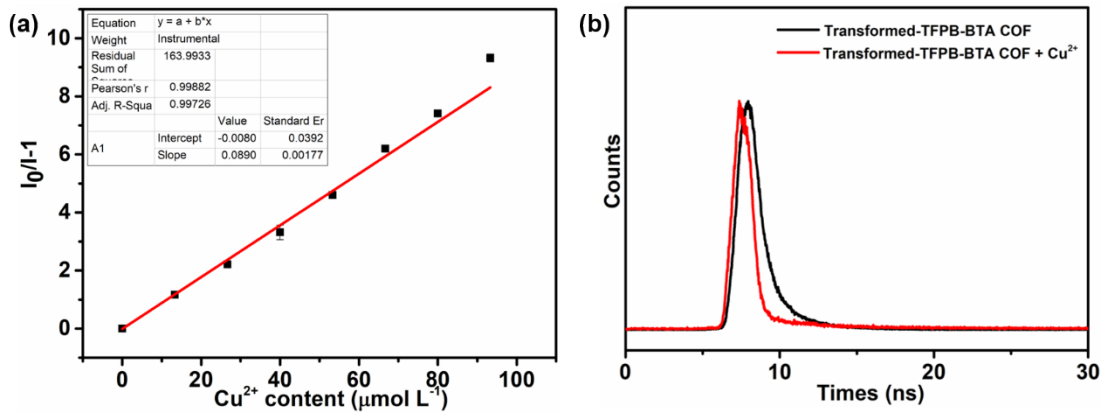

Fig. S26. (a) The linear correlation between the fluorescence change of the Transformed-TFPB-BTA COF and different concentrations of Cu^{2+} in EtOH (R^2=0.997), (b) fluorescence lifetime of the Transformed-TFPB-BTA COF before and after adding Cu^{2+}.

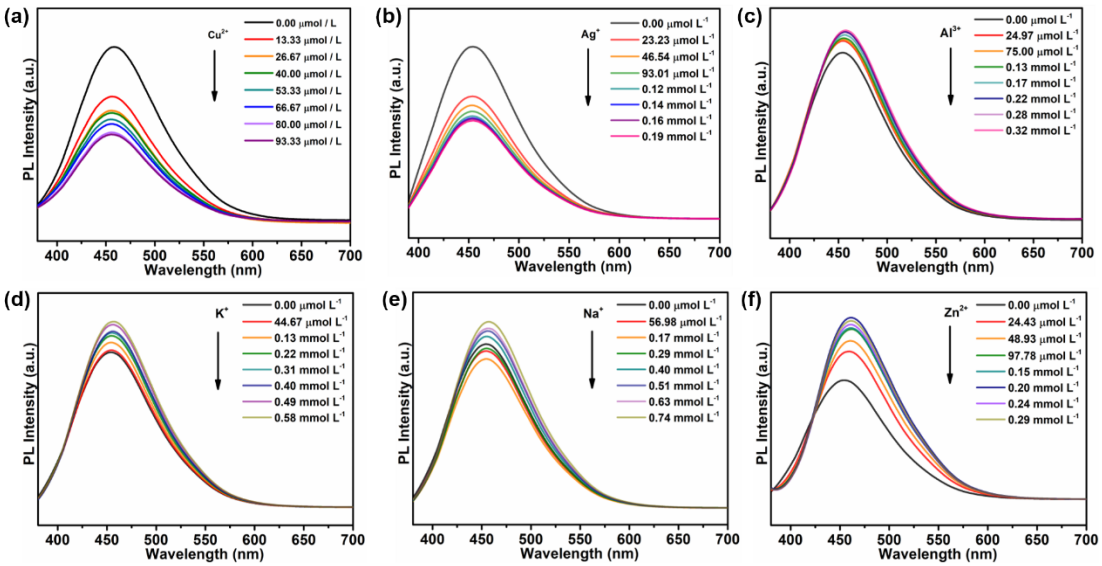

Fig. S27. Emission spectra of the Transformed-TFPB-DHz COF in EtOH suspensions containing various contents of (a) Cu^{2+}, (b) Ag^{+}, (c) Al^{3+}, (d) K^{+}, (e) Na^{+}, (f) Zn^{+}.

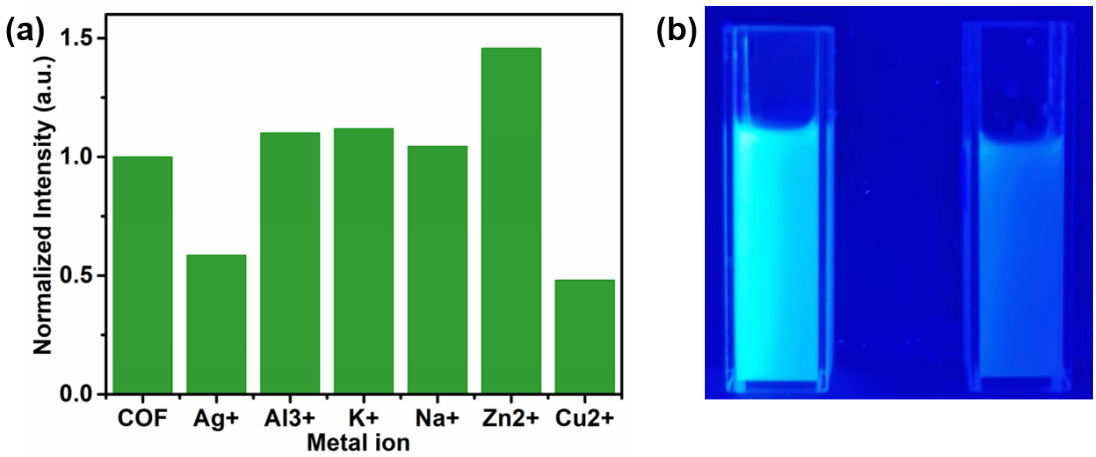

Fig. S28. (a) Comparison of the luminescence intensity of the Transformed-TFPB-DHz COF in the presence of various metal ions (0.17 mmol / L) in EtOH (λ_{ex} = 365 nm), (b) a photo showing fluorescence change (under a UV lamp with λ_{ex} = 365 nm) of the Transformed-TFPB-DHz COF in EtOH upon addition of 0.17 mmol / L of Cu^{2+}.

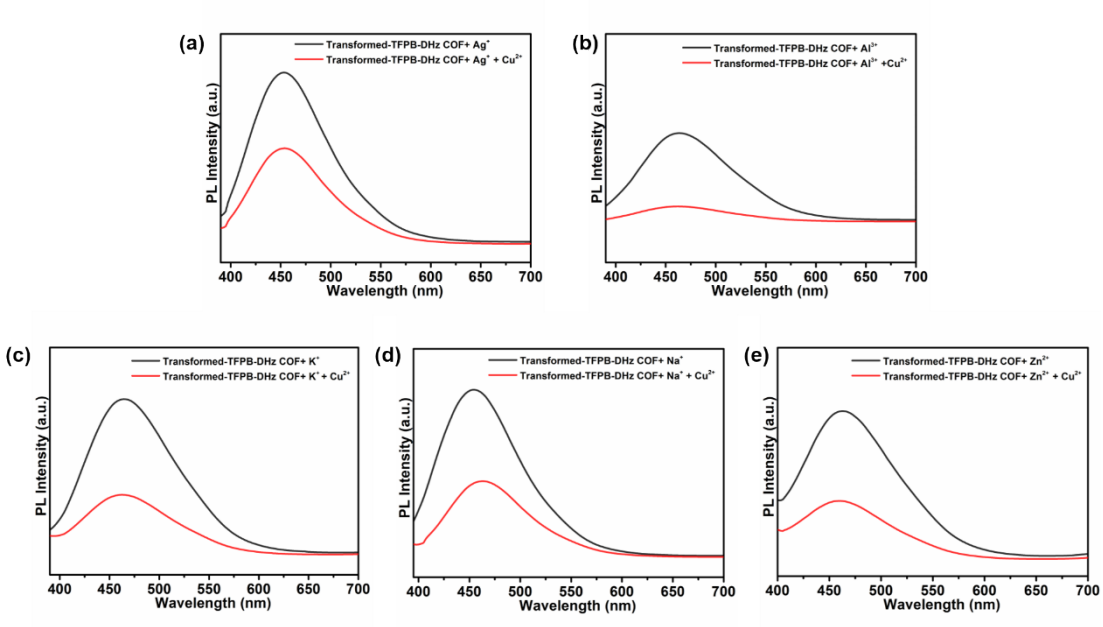

Fig. S29. Effect of different metal ions (100 mmol) on the detection of Cu^{2+} for the Transformed-TFPB-DHz COF.

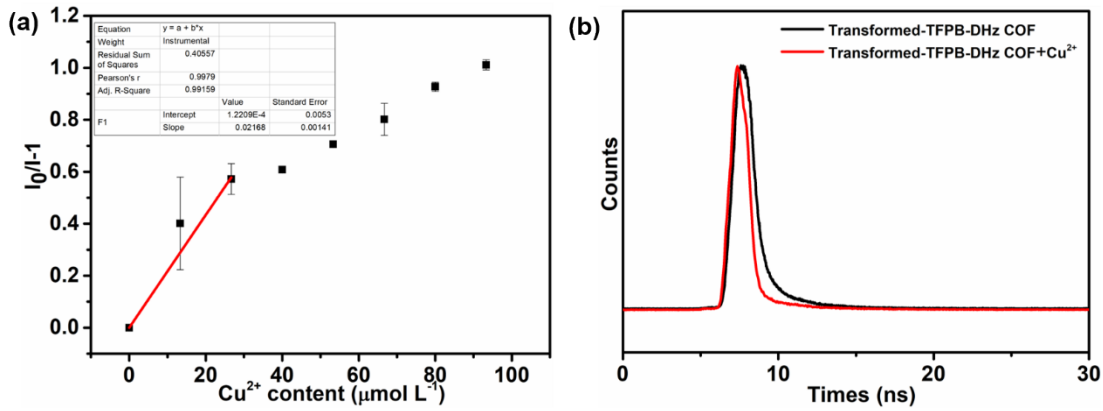

Fig. S30. (a) The linear correlation between the fluorescence change of Transformed-TFPB-DHz COF and different concentrations of Cu^{2+} in EtOH (R^2=0.992), (b) fluorescence lifetime of the Transformed-TFPB-DHz COF before and after adding Cu^{2+}.

Table S2. Atomic coordinates of the Transformed-TFPB-DETH COF for the AA-stacking mode.

Sample Name: Transformed-TFPB-DETH COF				
Space Group: P6				
a=44.94, b= 44.94, c= 3.82; α=β=90°, γ=120°				
R_{wp}=7.14%				
Atom	**type**	**x/a**	**y/b**	**z/c**

C1	C	0.40271	0.7603	-0.11393
C2	C	0.42066	0.79621	-0.10665
N3	N	0.43102	0.52498	-0.02081
N4	N	0.41292	0.54308	-0.0227
O5	O	0.47536	0.56413	-0.33886
C6	C	0.35614	0.75975	0.20977
C7	C	0.37377	0.79566	0.20907
C8	C	0.31516	0.68437	0.04458
C9	C	0.51922	0.48289	-0.17685
C10	C	0.29696	0.64824	0.04477
C11	C	0.37024	0.74145	0.04666
C12	C	0.40627	0.81416	0.054
C13	C	0.42465	0.85203	0.06106
C14	C	0.46362	0.48095	-0.17573
C15	C	0.462	0.53652	-0.18663
C16	C	0.48305	0.46433	-0.1814
O17	O	0.57242	0.53803	-0.20315
C18	C	0.58972	0.5702	-0.02291
C19	C	0.62434	0.5759	0.09687
H20	H	0.41397	0.74748	-0.25464
H21	H	0.44545	0.81005	-0.2347
H22	H	0.41995	0.50172	0.11246
H23	H	0.33193	0.74648	0.34801
H24	H	0.36242	0.80903	0.33902
H25	H	0.30112	0.69804	0.04485
H26	H	0.41128	0.86512	0.1494
H27	H	0.47001	0.43661	-0.19683
H28	H	0.57502	0.57051	0.21099
H29	H	0.59361	0.5914	-0.20183
H30	H	0.63929	0.57509	-0.12998
H31	H	0.62036	0.55515	0.28157
H32	H	0.63898	0.60108	0.23092

Table S3. Atomic coordinates of the Transformed-TFPB-BTA COF for the AA-stacking mode.

Sample Name: Transformed-TFPB-BTA COF				
Space Group: P6				
a=45.03, b= 45.03, c= 3.85; α=β=90°, γ=120°				
R_{wp}=7.14%				
Atom	**Type**	**x/a**	**y/b**	**z/c**

C1	C	0.4868	0.52259	1.19108
C2	C	0.46448	0.48697	1.19785
C3	C	0.47709	0.46404	1.20697
C4	C	0.47269	0.54615	1.17478
N5	N	0.55628	0.46213	0.99451
N6	N	0.5695	0.43974	0.98447
O7	O	0.51186	0.42572	1.32246
O8	O	0.54494	0.57115	1.19943
C9	C	0.57319	0.58466	1.4366
C10	C	0.60641	0.60022	1.24052
C11	C	0.62855	0.63392	1.24271
C12	C	-0.70231	-0.34694	-0.20933
C13	C	-0.68825	-0.36867	-0.20974
C14	C	-0.74026	-0.36146	-0.20522
C15	C	-0.5884	-0.24429	-0.36796
C16	C	-0.56628	-0.20883	-0.3589
C17	C	-0.57607	-0.18743	-0.19187
C18	C	-0.6084	-0.20209	-0.0325
C19	C	-0.63034	-0.23758	-0.03676
C20	C	-0.84945	-0.40216	-0.18572
H21	H	0.43706	0.47683	1.19529
H22	H	0.56847	0.48503	0.85376
H23	H	0.57223	0.56488	1.61566
H24	H	0.57178	0.60429	1.59923
H25	H	0.61276	0.5835	1.09509
H26	H	0.65237	0.64421	1.0983
H27	H	0.6232	0.65147	1.38625
H28	H	-0.70519	-0.39611	-0.20911
H29	H	-0.58033	-0.25976	-0.51006
H30	H	-0.54161	-0.19805	-0.4869
H31	H	-0.61655	-0.18623	0.10121
H32	H	-0.65442	-0.24794	0.10111
H33	H	-0.8599	-0.38836	-0.32194

Table S4. Atomic coordinates of the Transformed-TFPB-DHz COF for the AA-stacking mode.

Sample Name: Transformed-TFPB-DHz COF				
Space Group: P-6				
a=22.87, b= 22.87, c= 3.48; α=β=90°, γ=120°				
R_{wp}=15.04%				
Atom	**Type**	**x/a**	**y/b**	**z/c**
N1	N	0.14181	0.53924	0.5

N2	N	0.07193	0.51514	0.5
O3	O	0.16425	0.64609	0.5
C4	C	0.54854	0.41071	0.5
C5	C	0.52597	0.45733	0.5
C6	C	0.66388	0.50248	0.5
C7	C	0.64091	0.5488	0.5
C8	C	0.59783	0.31068	0.5
C9	C	0.95476	0.42807	0.5
C10	C	1.02767	0.45126	0.5
C11	C	0.61908	0.26241	0.5
C12	C	0.56831	0.18674	0.5
C13	C	0.37487	0.73813	0.5
C14	C	0.29254	0.59647	0.5
C15	C	0.18653	0.60746	0.5
H16	H	0.15852	0.50457	0.5
H17	H	0.50937	0.35867	0.5
H18	H	0.47213	0.43917	0.5
H19	H	0.71778	0.52445	0.5
H20	H	0.67741	0.60232	0.5
H21	H	0.54542	0.29343	0.5
H22	H	1.04418	0.41439	0.5
H23	H	0.26238	0.54218	0.5

Table S5. Elemental analysis results of the COFs.

COF		C%	H%	N%
TFPB-DETH COF	**Calcd.**	71.13	5.17	11.06
	Found	68.14	5.479	10.10
Transformed-TFPB-DETH COF	**Found**	69.29	5.419	10.21
TFPB-DHz COF	**Calcd.**	73.46	4.11	14.28
	Found	66.23	5.371	16.15
Transformed-TFPB-DHz COF	**Found**	64.47	5.664	14.02
TFPB-BTA COF	**Calcd.**	72.44	4.94	10.56
	Found	70.40	5.461	10.03
Transformed-TFPB-BTA COF	**Found**	70.73	5.549	9.96

Table S6. Comparison of different porous materials for Cu^{2+} detection.

Porous materials	Detection limit	Ions	Ref.
COPs-DT	0.076 μmol / L	Cu^{2+}	2
MOF-5-NH_2	0.057 μmol / L	Cu^{2+}	3

$[Eu_4(MTB)_3(DMF)_6].2DMF$	1.98 μmol / L	Cu^{2+}	4
$\{[Nd_2(NH_2\text{-}BDC)_3(DMF)_4]\}_n$	78.7 μmol / L	Cu^{2+}	5
TFPB-DHTH COF	12 nmol / L	Cu^{2+}	6
Transformed TFPB-DETH COF	**0.082 μmol / L**	**Cu^{2+}**	**This work**
Transformed TFPB-BTA COF	**0.26 μmol / L**	**Cu^{2+}**	
Transformed TFPB-DHz COF	**1.15 μmol / L**	**Cu^{2+}**	

Reference

1. S. Jiang, S. D. Liu, L. C. Meng, Q. K. Qi, L. P. Wang, B. Xu, J. Q. Liu and W. J. Tian, *Science China-Chemistry*, 2020, **63**, 497-503.
2. C. Cui, Q. Wang, C. Xin, Q. Liu, X. Deng, T. Liu, X. Xu and X. Zhang, *Microporous Mesoporous Materials*, 2020, **299**, 110122.
3. X. X. An, Q. Tan, S. Pan, H. Liu and X. L. Hu, *Spectrochimica Acta Part A-Molecular and Biomolecular Spectroscopy*, 2021, **247**, 119073.
4. J. Luo, B. S. Liu, Y. C. Zhang, B. K. Wang, B. B. Guo, L. She and T. H. Chen, *Journal of Molecular Structure*, 2023, **1274**, 134460.
5. J. Luo, B. S. Liu, C. Cao, F. Wei, *Inorganic Chemistry Communications*, 2017, **76**, 18−21.
6. L. R. Ahmed, A. F. M. EL-Mahdy, C. T. Pan, and S. W. Kuo, *Materials Advances*, 2021, **2**, 4617-4629.